

# DESIGN OF A SPIRAL INFLECTOR AT iTHEMBA LABS FOR INJECTING THE BEAM INTO A CYCLOTRON

A. H. Barnard<sup>†</sup>, iThemba Laboratory for Accelerator Based Sciences, Cape Town, South Africa

## Abstract

Using a Belmont-Pabot spiral inflector for axial beam injection presents difficulties when matching the beam emittance to the cyclotron acceptance. For an electrostatic inflector one of the potential solutions to this problem is to use transverse electric field gradients to influence and optimise the optics. Here we extend this approach to magnetic spiral inflectors. It is demonstrated that the gradient of the magnetic field along the central trajectory can be controlled by an appropriate permanent magnet inflector design, and that these gradients have a large influence on the optics. The transverse gradients are numerically optimised and the performance compared to an optimised electrostatic spiral inflector. A faster numerical method for accurately determining the electric field of an electrostatic inflector is also presented.

## INTRODUCTION

Traditional Belmont-Pabot spiral inflectors suffer from a large vertical divergence, and in addition to this the transverse-longitudinal coupling results in a de-bunching longitudinal spread [1]. Both of these issues decrease the transmission of the cyclotron. Recent attempts at addressing these problems at several cyclotron facilities have made use of transverse electric field gradients along the central path to attempt to influence the optics and focus the beam [2-5]. In previous work [1] we have shown that in the most general case the electric potential can be described, to second order in the transverse displacements, by:

$$\phi = -u_r E_0 - Q_1 E_0 \frac{u_r^2 - h_r^2}{2} - Q_2 E_0 h_r u_r - \frac{u_r^2}{2} \hat{s}' \cdot \mathbf{E}_0$$

Where  $Q_1(s)$  and  $Q_2(s)$  are quadrupole parameters, and may be freely selected by an inflector designer. The coordinates  $(u_r, h_r, s)$  are the standard rotated coordinates used in spiral inflector design, where the electric field points in the  $\hat{u}_r$  direction. The corresponding electric fields are then:

$$E_{u_r} = E_0 + u_r(Q_1 E_0 + \hat{s}' \cdot \mathbf{E}_0) + h_r Q_2 E_0 \quad (1a)$$

$$E_{h_r} = u_r Q_2 E_0 - h_r Q_1 E_0 \quad (1b)$$

$$E_s = u_r E_0' - h_r \kappa_s E_0 \quad (1c)$$

By numerically optimising the two free quadrupole parameters  $Q_1(s)$ ,  $Q_2(s)$  an inflector design was obtained that showed good vertical and longitudinal performance. This device was constructed and experimentally shown to improve the transmission through the Solid Pole Cyclotron 2 (SPC2) at iThemba LABS by 60%.

In this article the application of a similar optimisation process to a permanent magnet spiral inflector is presented.

## FASTER NUMERICAL METHOD

Optimisation of an electrostatic inflector design involves repeated numerical computations of the electric field, for a great number of proposed inflectors. This was previously done using TOSCA, which required about an hour per inflector. To speed this up in the past a method was used to estimate the electric field, by combining the results from a number of pre-calculated TOSCA simulations and linearly extrapolating [5]. This method could compute the transfer matrix of a new inflector within about 5 seconds, but lacked accuracy.

A new numerical method was therefore developed that is able to accurately compute the inflector transfer matrix in a short time (about 4 seconds). It is based on calculating the surface charge density on the inflector electrodes, by minimising the potential energy.

Suppose that the inflector surface has been divided into approximate squares, of side length  $L_i$  and containing a charge  $q_i$  per square. Such a meshing of the electrodes is shown in Fig. 1.

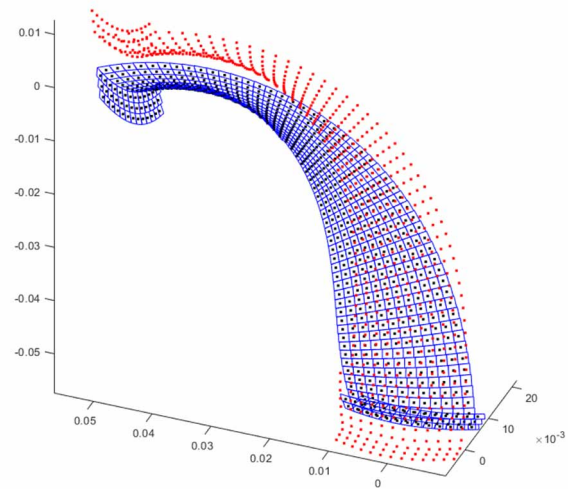


Figure 1: Square meshing of the negative electrode, also showing the centroids of the squares on both electrodes.

The total potential energy can be expressed as:

$$U = \frac{1}{2} \mathbf{q} \cdot \mathbf{V}_q + \mathbf{q} \cdot \mathbf{V}_E$$

Where  $\mathbf{V}_q$  is the voltage due to the surface charges and  $\mathbf{V}_E$  is an externally applied voltage. We write the voltage as  $\mathbf{V}_q = D\mathbf{q}$  where:

$$D_{ij} = \frac{f_{ij}}{4\pi\epsilon_0|\mathbf{r}_i - \mathbf{r}_j|}$$

<sup>†</sup>hbarnard@tlabs.ac.za

Here  $\mathbf{r}$  is the location of the centre of the square, and  $f_{ij}$  is a geometric factor to account for the finite size and relative orientation of the squares. As the squares become smaller we can set  $f_{ij} = 1$ . This is done for all squares, except where  $i = j$ , in which case the self-energy of a square results in:

$$D_{ii} = \frac{2}{4\pi\epsilon_0 q_i^2} \iint \frac{1}{|\mathbf{r}_1 - \mathbf{r}_2|} dq_1 dq_2 \approx 2 \frac{1.4865}{4\pi\epsilon_0 L_i}$$

The total charge on electrode  $n$  is fixed to be  $Q_n$ , and this constraint is enforced using the Lagrange multiplier  $\lambda_n$ . To help with this we introduce the electrode indicator  $c_i^n$  which is 1 if square  $i$  is in electrode  $n$ , and zero otherwise. The optimisation problem becomes:

$$\min \frac{1}{2} \mathbf{q} \cdot D\mathbf{q} + \mathbf{q} \cdot \mathbf{V}_E + \lambda_1 \mathbf{q} \cdot \mathbf{c}^1 + \dots + \lambda_N \mathbf{q} \cdot \mathbf{c}^N$$

The solution is:

$$D\mathbf{q} + \mathbf{V}_E + (\lambda_1 \mathbf{c}^1 + \dots + \lambda_N \mathbf{c}^N) = 0$$

But note that  $D\mathbf{q} + \mathbf{V}_E$  is in fact the total voltage  $\mathbf{V}$ , so the Lagrange multiplier is just negative of the voltage on an electrode  $\lambda_n = -V^n$ , and the surface charge per square is obtained from:

$$\mathbf{q} = D^{-1}(\mathbf{V} - \mathbf{V}_E)$$

These surface charges  $\mathbf{q}$  are computed first, and then stored. During run-time, when tracing the path of a particle through the inflector, the electric field at  $\mathbf{x}$  is computed as:

$$\mathbf{E}(\mathbf{x}) = \frac{1}{4\pi\epsilon_0} \sum_i q_i \frac{\mathbf{x} - \mathbf{r}_i}{|\mathbf{x} - \mathbf{r}_i|^3}$$

With the caveat that the distance to the closest surface charge should not be too small. In practice this limit is found to be about twice the largest value of  $L_i$ .

This surface charge method was tested in several simple cases with known analytical solutions. For a parallel plate capacitor, the error in the electric field between the plates was 0.5%. The induced surface charge on a flat earthed plate due to the presence of an external test charge was computed to within 1%. A comparison of this method with TOSCA is provided in Fig. 2, where they correspond quite well.

## MAGNETIC SPIRAL INFLECTOR

The use of permanent magnets to construct a magnetic spiral inflector has been proposed in the past [6]. An advantage of such a magnetic inflector is that higher injection energies can be achieved than with an electric inflector, which will reduce the impact of space-charge in the inflector. Here we investigate a magnetic inflector (in the absence of space charge for now), to see if it can be optimised in a similar way to the electric inflector, by creating quadrupole fields along the central path.

The magnetic field is selected so that the force on the central path due to the permanent magnets is the same as the electric force in an electric inflector:

$$\mathbf{E} = E_0 \hat{u}_r \rightarrow \mathbf{B} = -\frac{E_0}{v} \hat{h}_r$$

The magnetic field is produced by a number of modified Halbach rings, which are known to create a strong internal magnetic field and a much weaker external field. Figure 3 shows such an inflector and Fig. 4 shows the numerically measured field on the central path.

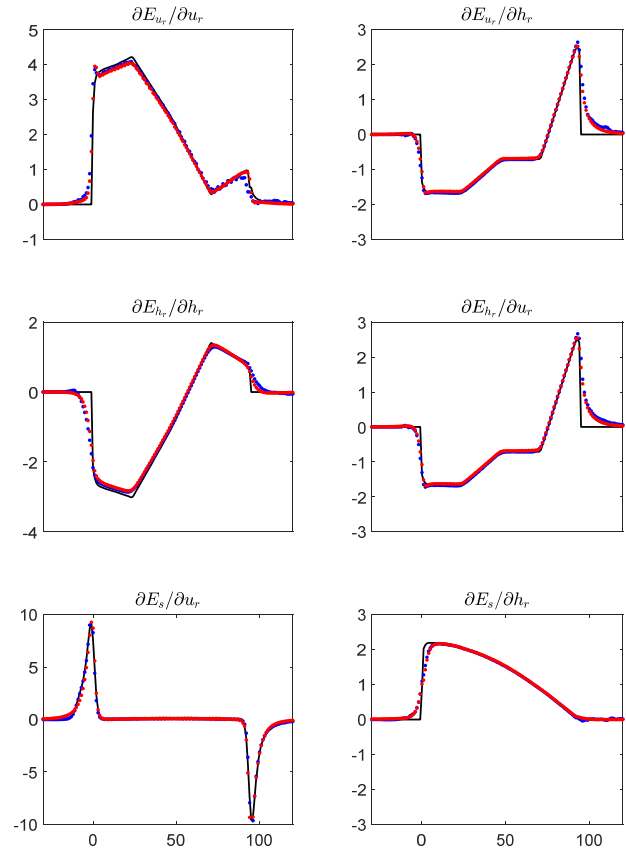


Figure 2: The field gradients of an inflector as computed using: TOSCA (blue dots), the surface charge method presented here (red dots), and the analytical approximation via Eq. (1) (black solid line).

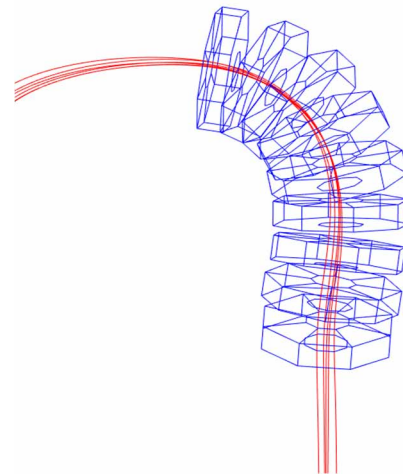


Figure 3: The magnetic inflector made of 8-sided Halbach rings.

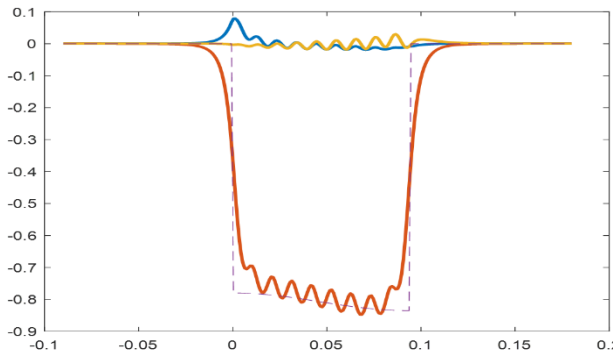


Figure 4: The magnetic field (T) along the central path (m).  $B_{u_r}$  is blue,  $B_{h_r}$  is red and  $B_s$  is yellow. The oscillations are due to the discrete number of rings.

The internal field of the Halbach ring is a function of the magnetisation of the ring segments. By using 8-sided rings, it is possible to create quadrupoles along the central path, as shown in Fig. 5. The radial and azimuthal components of the magnetisation of the ring can then be expressed as:

$$M_r = M_0(\sin \theta - K_1 \cos 2\theta - K_2 \sin 2\theta)$$

$$M_\theta = M_0(-\cos \theta - K_1 \sin 2\theta + K_2 \cos 2\theta)$$

Where  $\theta$  refers to the azimuthal angle of the centre of each of the 8 segments, and  $K_1$  and  $K_2$  are quadrupole parameters.

The magnetic field due to the inflector only can be computed from the gradient of the scalar potential  $\psi$ . This is similar to the electric case, and by analogy this can be expressed as:

$$\psi = h_r B_0 - Q_1 B_0 \frac{u_r^2 - h_r^2}{2} - Q_2 B_0 u_r h_r - \frac{u_r^2}{2} \hat{s}' \cdot \mathbf{B}_0$$

Giving the fields to first order in the displacements  $u_r, h_r$ :

$$B_{u_r} = u_r(Q_1 B_0 + \hat{s}' \cdot \mathbf{B}_0) + h_r Q_2 B_0 \quad (2a)$$

$$B_{h_r} = -B_0 + u_r Q_2 B_0 - h_r Q_1 B_0 \quad (2b)$$

$$B_s = -h_r B'_0 + u_r \kappa_s B_0 \quad (2c)$$

These expressions were confirmed by numerically evaluating the fields, as shown in Fig. 6. Note that  $Q_1, Q_2$  which describe the quadrupole nature of the magnetic fields, are almost proportional to  $K_1, K_2$  which describe the

magnetisation of the Halbach rings, but the exact relationship depends on the size of the rings and their placement along the central path.

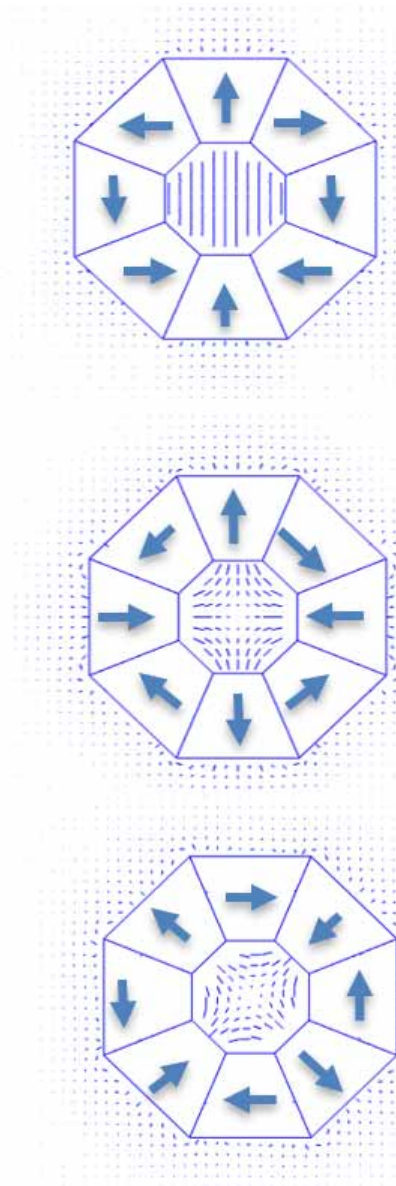


Figure 5: Magnetisation of the rings to produce a dipole field (top) and normal and skew quadrupole fields (middle and bottom).

Content from this work may be used under the terms of the CC-BY-4.0 licence © 2022. Any distribution of this work must maintain attribution to the author(s), title of the work, publisher, and DOI

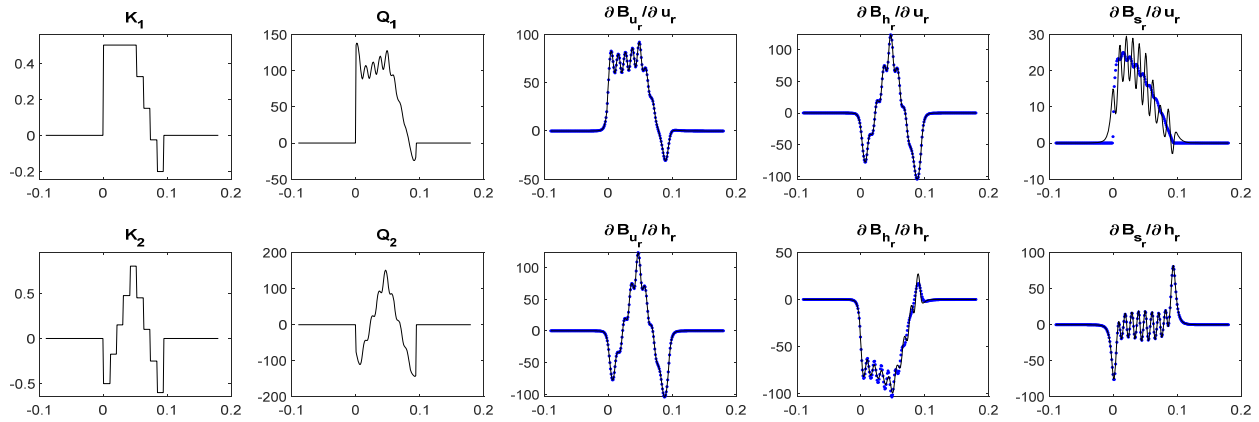


Figure 6: Numerical verification of Eq. (2), showing various properties plotted against the inflector path length (m). From left to right: 1) The K values use to design the Halbach rings. 2) The resulting Q values describing the quadrupole fields. 3) Gradients of  $B_{u_r}$ , with numerical values in blue and Eq. (2) in black. 4) Gradients of  $B_{h_r}$ . 5) Gradients of  $B_s$ .

### OPTIMISATION

The aim was to optimise the transmission of the beam through the SPC2 cyclotron at iThemba LABS. In the past the acceptance of the cyclotron was not known, and hence the optimisation only aimed to limit the vertical and longitudinal emittance and spread [1, 5]. For this reason, a new numerical model of the SPC2 was created to evaluate its acceptance.

The magnetic fields were partly obtained from a full 3D TOSCA simulation of the cyclotron [7]. The electric field was based on a numerical solution of the electric field in the acceleration gap. Trim coils, based on TOSCA simulations, were added to obtain isochronism. The central trajectory was found by injecting a particle backwards from extraction, along an accelerated equilibrium orbit, and this trajectory corresponded well to the original central path calculated by the designers of SPC2. The main losses were radially on the slits in the central region and vertically on the slits and the dees.

It was found that an ellipse poorly represented the complex acceptance shape in phase space. A better representation of the acceptance was to select and number ( $\sim 10^4$ ) of random points inside the acceptance and to replace each point with a ball of constant radius in phase space. The volume occupied by these balls was then a better representation of the acceptance, and testing if a new point lay inside the acceptance is very quick.

The inflector simulation started in the axial hole in the yoke where the magnetic field is zero, and ends in the region between the inflector exit and the first acceleration gap, where the electric field is almost zero.

The injected beam is focussed at the inflector entrance, and a first harmonic buncher is used. The voltage of the buncher is set so it focusses at the first acceleration gap, which requires accounting for the optical length of the inflector ( $R_{56}$ ).

To compute the transmission of the beam through SPC2 when using a specific inflector, the procedure was:

1. Compute the linear transfer matrix of the inflector  $R$
2. Select a random particle in the DC beam upstream of the buncher
3. Propagate to the start of the inflector calculation (not linear in time due to sinusoid in buncher)
4. Transfer the particle through the inflector using its linear transfer matrix  $R$
5. Check if the particle is in the cyclotron acceptance
6. Go back to 2 and repeat for  $\sim 1e5$  particles

### RESULTS

The optimisation space for the electric inflector was the two functions  $Q_1(s)$  and  $Q_2(s)$ . For the magnetic inflector it was the  $K_1(n)$ ,  $K_2(n)$  parameters that had to be selected for each ring  $n$ . The optimal designs are shown in Fig. 7-8. Table 1 shows the transmission through SPC2 before and after optimisation, where the non-optimised inflector refers to the  $K = 0$  case for magnetic deflectors, and the  $Q = 0$  case for electric deflectors.

Table 1: Transmission through the Cyclotron

	Electric	Magnetic
Non-optimised	26%	33%
Optimised	43%	45%
Relative Improvement	65%	36%

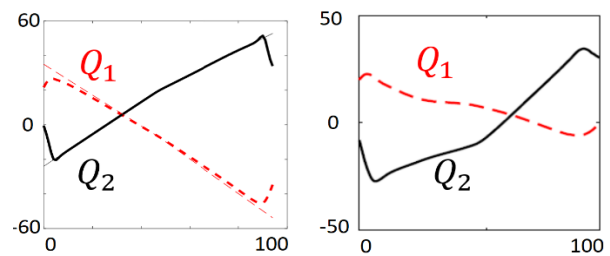


Figure 7: Quadrupole parameters ( $m^{-1}$ ) vs path length (mm). The optimal design for the electric inflector in this work (left) and a comparison with previous work in [1] (right).

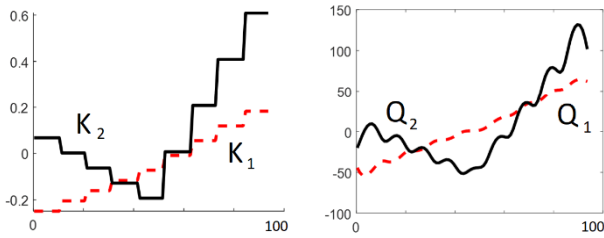


Figure 8: The optimal design of the magnetic inflector vs the path length (mm). Left: the ring magnetisation  $K$  values (unitless). Right:  $Q$  values ( $\text{m}^{-1}$ ) of the resultant quadrupole fields.

## DISCUSSION

In both the magnetic and electric case there is a substantial improvement when optimising the design. The final transmission of the electric and magnetic inflectors is similar. Note that the actual transmission through the SPC2 cyclotron is typically 5%, which is much less than these calculated values. This is partly because we have not accounted for losses at extraction yet (known to be a factor of about 3) and the emittance of the injected beam is also uncertain. This is to be investigated in further work in the future.

## CONCLUSION

The magnetic inflector can be optimised in a similar way to the electric inflector, by creating quadrupole fields in the transverse plane.

## REFERENCES

- [1] A.H. Barnard *et al.*, “Longitudinal and vertical focusing with a field gradient spiral inflector,” *Phys. Rev. Accel. Beams*, vol. 24, Feb. 2021, pp. 023501.  
doi:10.1103/PhysRevAccelBeams.24.023501
- [2] I. A. Ivanenko, “The Methods of Compensation of the Beam Vertical Divergence at the Exit of Spiral Inflector in Cyclotrons,” in *Proc. Cyclotrons'16*, Zurich, Switzerland, Sep. 2016, pp. 221-223.  
doi:10.18429/JACoW-Cyclotrons2016-TUP25
- [3] V. L. Smirnov, “Central Region Design in a Compact Cyclotron,” *Phys. Part. Nucl. Lett.*, vol 16, Apr. 2019, pp. 34-45.  
doi:10.1134/S1547477119010114
- [4] H. Tsutsui, “Accelerator and Cyclotron,” European Patent Office EP2391190A2, JP 2010120716, May 2010.
- [5] A. H. Barnard *et al.*, “Vertical Focussing with a Field Gradient Spiral Inflector,” in *Proc. Cyclotrons'19*, Cape Town, South Africa, Sep. 2019, pp. 58-61.  
doi:10.18429/JACoW-CYCLOTRONS2019-MOP016
- [6] L. Calabretta *et al.*, “Review of High-Power Cyclotrons and Their Applications,” in *Proc. Cyclotrons'19*, Cape Town, South Africa, Sep. 2019, pp. 289-293.  
doi:10.18429/JACoW-CYCLOTRONS2019-THB01
- [7] J. G. De Villiers *et al.*, “Numerical Orbit Tracking in 3D Through the Injector Cyclotron for Heavy Ions at iThemba LABS,” in *Proc. Cyclotrons'16*, Zurich, Switzerland, Sep. 2016, pp. 71-74.  
doi:10.18429/JACoW-Cyclotrons2016-MOP10

Content from this work may be used under the terms of the CC-BY-4.0 licence (© 2022). Any distribution of this work must maintain attribution to the author(s), title of the work, publisher, and DOI